

Measurement of intrinsic alignments in galaxy ellipticities

M.L. Brown¹, A.N. Taylor¹, N.C. Hambly¹ & S. Dye²

¹ *Institute for Astronomy, University of Edinburgh, Royal Observatory, Blackford Hill, Edinburgh, U.K.*

² *Astrophysics Group, Blackett Lab, Imperial College, Prince Consort Road, London, U.K.*

mlb@roe.ac.uk, ant@roe.ac.uk

20 May 2019

ABSTRACT

We measure the alignment of galaxy ellipticities in the local universe over a range of scales using digitized photographic data from the SuperCOSMOS Sky Survey. We find for a magnitude cut of $b_J < 20.5$, corresponding to a median galaxy redshift of $z \approx 0.1$, and 1.7×10^6 galaxies, that the galaxy ellipticities exhibit a non-zero correlation over a range of scales between 1 and 100 arcminutes. In particular, we measure the variance of mean galaxy ellipticities, $\sigma^2(\theta)$, in square angular cells on the sky as a function of cell size and find it lies in the range, $1 \times 10^{-2} \geq \sigma^2(\theta) \geq 3 \times 10^{-5}$ for cell side lengths between $1 \leq \theta \leq 100$ arcminutes. Considering the low median redshift of the galaxies in the sample and hence the relatively low effective cross-section for lensing of these galaxies by the large-scale structure of the Universe, we propose that we have detected an intrinsic alignment of galaxy ellipticities. We compare our results to recent analytical and numerical predictions made for the intrinsic galaxy alignment and find good agreement. We discuss the importance of these results for measuring cosmic shear from upcoming shallow surveys (e.g. Sloan Digital Sky Survey) and we outline how these measurements could possibly be used to constrain models of galaxy formation and/or measure the mass distribution in the local universe.

Key words: cosmology: observations - gravitational lensing - large-scale structure, galaxies: formation

1 INTRODUCTION

Over the last decade, considerable interest has been directed towards the measurement and analysis of galaxy ellipticities as a means to estimate shear induced by gravitational lensing (see e.g. Bartelmann & Schneider 1999). On the scale of galaxy clusters, this is now a well-established method, with tools to invert the shear pattern and measure the distribution of Dark Matter. Recently attention has moved to larger scales to measure the cosmological weak shear signal of lensing by large-scale structure and a number of groups have made consistent detections (Bacon, Refregier & Ellis 2000; Kaiser, Wilson & Luppino 2000; van Waerbeke et al. 2000; Wittman et al. 2000). Despite the remarkable success of the shear analysis, up until recently very little attention had been paid to the prospect of intrinsic alignments mimicking the gravitational shear signal. The most likely ways for this to occur is during the tidally induced spin-up of galaxies (Hoyle 1949), where the angular momentum axes, and hence ellipticities, are aligned, or through the alignment of galaxy and halo shapes.

Over the last year, this problem has been addressed by a number of groups using a combination of numerical (Heavens, Refregier & Heymans 2000, Croft & Metzler 2000)

and analytic methods (Catelan, Kamionkowski & Blandford 2000, Crittenden et al 2000). Although these results are in rough agreement, a complete understanding of alignments is less secure, with the main problems lying in understanding the coupling of the tidal and inertial tensors of dark matter haloes, and the alignment of galaxies and haloes. On the observational side Pen, Lee & Seljak (2000) have recently claimed a weak detection of spin-spin correlations in the Tully catalogue. In this letter we have measured the variance of ellipticities of galaxies at low-redshift, where the effect of intrinsic alignments is predicted to be orders of magnitude higher than a lensing effect. These observations may help to distinguish between models for alignments.

This letter is laid out as follows. In Section 2 we present the observational material used in the analysis. In Section 3 the main analysis methods are introduced, and our results are presented in Section 4, where we discuss the significance of our results. Our conclusions are presented in Section 5.

2 OBSERVATIONAL MATERIAL

The observations analysed in this letter are taken from the SuperCOSMOS Sky Survey program (Hambly et al. 2000a).

This digitised photographic sky survey is being undertaken using Schmidt photographic sky atlas plates, and currently covers ≈ 5000 square degrees (200 individual Schmidt fields) at high Galactic latitude in the southern hemisphere (the so-called South Galactic Cap, or SGC, survey region)*.

We have constructed an object catalogue (including both stars and galaxies) for the SGC region by pairing the scanned b_J and R plates. Apart from a small number of large overlap regions near the 0^h boundary in the survey which were used for internal consistency checks (see Section 3.3), we created a ‘seamless’ catalogue from the overlapping plates using the scheme described in Hambly et al. (2000a). This scheme attempts to include the image with the best parameters (and exclude the others) when there is a choice to be made for the same image appearing on more than one plate. Pairing the b_J and R plates has the advantage over single-colour catalogues in that spurious objects on one plate are eliminated. This is particularly important for galaxy studies from Schmidt photographs since these defects are broken up into many co-aligned ‘galaxies’ by the image analyser. Such a large source of contaminants could potentially ruin any shear analysis.

Regions around bright stars and blended (ie. multiple) images have been excluded from the object catalogue to further eliminate spurious and/or poorly parameterised images. Further details concerning image parameterisation, classification and photometry are given in Hambly et al. (2000b). Image parameters included in the final object catalogue generated for this study consisted of celestial co-ordinates, local plate co-ordinates, intensity-weighted second-order moments (semi-major/minor axes and celestial position angle), b_J magnitude, (b_J -R) colour, image classification flag and stellarness index. The external reliability of the image classification on the J plates is demonstrated in Hambly et al. (2000b) as $\geq 92\%$ reliable for $b_J \leq 20.5$ with completeness at around $\sim 97\%$. Photometric accuracy for galaxies is around 0.25 mag. The internal consistency and accuracy in image ellipticity parameters is demonstrated later in Section 3.3.

3 ANALYSIS METHODS

In order to measure the intrinsic alignments of galaxies, we first divide the survey into square cells of angular side length, θ . We define the mean ellipticity of galaxies within each cell, e_i , as

$$\begin{aligned} \bar{e}_{1,i} &= \frac{1}{N} \sum_{j=1}^N e_{1,j}, & \bar{e}_{2,i} &= \frac{1}{N} \sum_{j=1}^N e_{2,j}, \\ e_i^2 &= \bar{e}_{1,i}^2 + \bar{e}_{2,i}^2, \end{aligned} \quad (1)$$

where N is the number of galaxies in the i^{th} cell and $e_{1,j}$ and $e_{2,j}$ are the ellipticity components of the j^{th} galaxy which are defined with respect to the cell axes as

$$e_{\alpha,j} = \frac{a_j^2 - b_j^2}{a_j^2 + b_j^2} \begin{cases} \cos 2\varphi_j & \alpha = 1 \\ \sin 2\varphi_j & \alpha = 2 \end{cases}. \quad (2)$$

* Full details and online access to the data are available via the World Wide Web at URL <http://www-wfau.roe.ac.uk/sss>

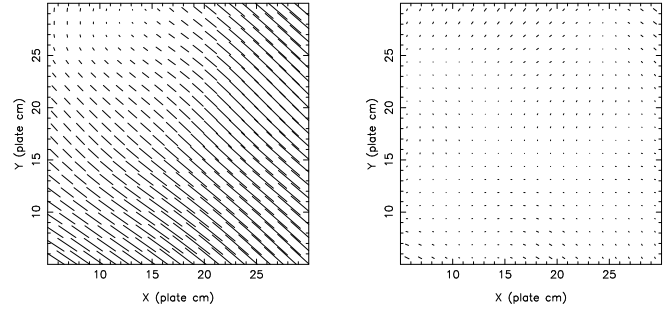


Figure 1. Ellipticity fields across a plate for raw (LHS) and corrected (RHS) stars for one of the SGC fields. Stars are binned into cells of a side $10'$ and smoothed with a Gaussian with a smoothing scale $25'$. For both plots, the length of each vector drawn is 25 cm times the measured cell ellipticity. The average ellipticity in a cell in the raw field is $\bar{e} \approx 10^{-2}$, while the average ellipticity in a corrected cell across the plate is $\bar{e} \approx 10^{-4}$.

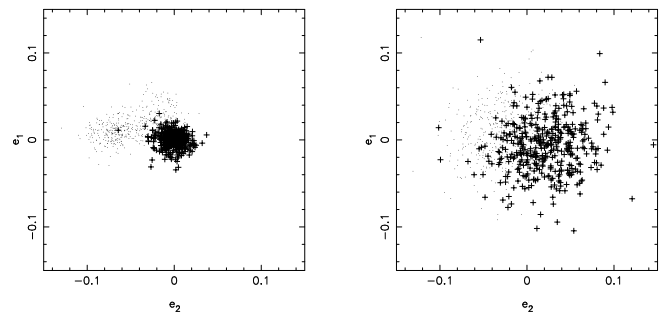


Figure 2. Ellipticity distribution on a plate per cell (stars on the left, galaxies on the right) for one of the SGC fields. The dots are the raw stars/galaxies, the crosses the corrected values. Each cell has an ellipticity estimated from equation (1) and has an uncertainty given by equation (8). For this plate, raw stars have a mean ellipticity, averaged over all cells in the plate of $\bar{e}_1 = 1.6 \times 10^{-2}$ and $\bar{e}_2 = -5.0 \times 10^{-2}$. After subtraction, the stars have $\bar{e}_1 = -2.3 \times 10^{-4}$ and $\bar{e}_2 = -1.3 \times 10^{-3}$.

Here, a and b are the semi-major and semi-minor axes of the galaxy and φ is the orientation of the semi-major axis with respect to the cell axes. To quantify the degree of alignment of the cell ellipticities, we calculate the variance of e_i on a given scale across the entire survey. Since this statistic has been used to measure cosmic shear (e.g. Bacon et al., 2000, Kaiser et al., 2000), we can directly compare the contributions of intrinsic and extrinsic galaxy alignments. In order to obtain an accurate estimate of e_i for a cell, a number of corrections to the raw image catalogue are required. We now describe the sources of error on the ellipticity measurements of galaxies and the corrections we have applied to the dataset.

3.1 Correction for plate distortions and PSF anisotropy

There are large-scale plate distortions on all the plates scanned due to the manner in which the plates are mounted on the telescope during observing, and additional distortions introduced by anisotropy in the point spread function (PSF). These distortions result in spurious ellipticities for all the objects detected and must be removed before a shear

analysis can be performed. We have done this by comparing with the ellipticity field for the stars. Stars should have no intrinsic ellipticity and so the measured stellar ellipticities are due to plate distortions. To correct the galaxy ellipticities, the plates are gridded up and an average stellar ellipticity is calculated for each cell in the grid. This ellipticity field is then Gaussian smoothed across the plate. If the grid used for smoothing is too small, a coherent distortion pattern cannot be made and an essentially random pattern is generated. Due to the different response of stellar point sources and extended galaxy images to a PSF “smear” distortion, simply subtracting the smoothed average stellar ellipticity field from each galaxy over-corrects the galaxy ellipticities, producing a spurious signal. We therefore empirically recalibrate the correction for the galaxies before subtraction, to remove this effect.

Figure 1 illustrates the stellar ellipticities on a plate before and after this correction. A strong, coherent distortion of $\bar{e} \approx 10^{-2}$ is corrected to produce a random ellipticity pattern with mean $\bar{e} \approx 10^{-4}$. Figure 2 shows a scatter plot of the ellipticities (e_1 vs. e_2) for both stars (LHS) and galaxies (RHS) before (dots) and after (crosses) correction. Each point corresponds to a cell, with an ellipticity value given by equation (1), and an uncertainty given by equation (8).

3.2 Seeing correction

The effect of seeing on the galaxy ellipticities is to circularize the images, causing a decrease in ellipticities. The seeing across all of the plates is typically $2''$. This is comparable to the size of a galaxy near the magnitude limit of our survey ($b_J < 20.5$) and thus, needs to be corrected for before the galaxy ellipticities can be trusted.

We assume that the semi-major and semi-minor axes of each galaxy transforms under the effect of seeing as

$$a'_j{}^2 = a_j^2 + r_i^2, \quad b'_j{}^2 = b_j^2 + r_i^2, \quad (3)$$

where (a_j, b_j) and (a'_j, b'_j) are the axes of the j^{th} galaxy before and after the effect of seeing respectively and r_i is the average seeing in the i^{th} plate. The effect of seeing on the measured ellipticities is

$$e'_{\alpha,j} = f_{ij} e_{\alpha,j}, \quad (4)$$

where $e'_{\alpha,j}$ is the post-seeing ellipticity and we have defined a “seeing factor” which is, in terms of the observed semi-major and semi-minor axes,

$$f_{ij} = 1 - \frac{2r_i^2}{a_j'^2 + b_j'^2}. \quad (5)$$

The uncertainty on individual galaxy sizes was too large to use equation (4) directly. Instead we estimated an effective galaxy size for all plates for a give flux cut, calibrated by matching ellipticities in a number of plate overlap regions. In the case of $b_J \leq 20.5$, this was $2.5''$, which closely matched the directly measured mean galaxy size. This was then used to correct all the plates, using the measured seeing from each plate.

3.3 Internal consistency tests

We have tested for internal consistency in the dataset by comparing ellipticity measurements on regions of the sky

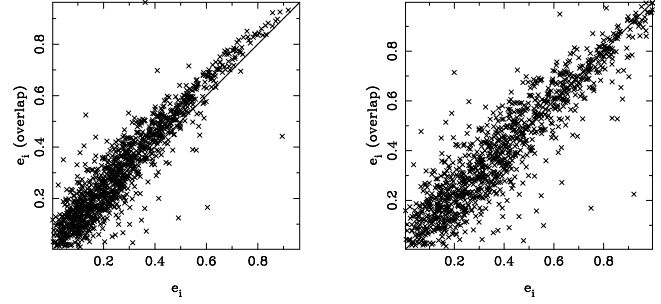


Figure 3. Individual galaxy ellipticities measured from overlapping SGC fields. The left-hand panel shows the ellipticity measurements before the seeing correction is applied. The plate plotted on the horizontal scale has greater seeing than the plate plotted on the vertical axis. The right hand panel shows the ellipticities after the correction.

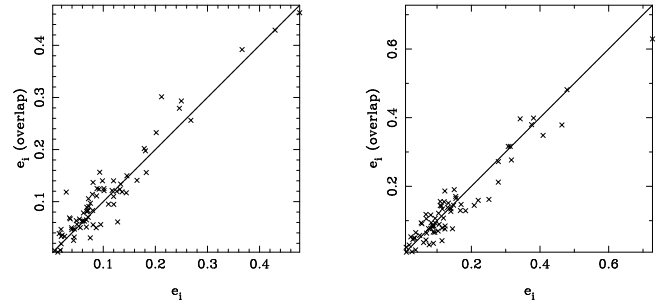


Figure 4. Binned cell ellipticities, e_i measured from the same plates as shown in Figure 3. The left-hand and right hand panel are the measurements before and after the seeing correction is applied respectively.

where plates overlap. The ellipticity measurements for a galaxy in an overlap region as measured on the two overlapping plates should agree to within the limits of the measuring process (the measurement errors are dominated by noise on the original photographs) assuming that we have corrected for the effect of seeing accurately enough.

Figures 3 and 4 show the correlation between different plates in the overlap region, after correction for plate distortions, for individual galaxies (Fig. 3) and binned cells (Fig. 4). The left-hand-side of Figures 3 and 4 show the correlation before correcting for seeing. There is an apparent decrease in the ellipticities of the galaxies plotted on the horizontal axis, where the seeing on the plate is larger. The right-hand-side of Figures 3 and 4 show the correlation after correction for seeing. As we are only scaling ellipticities the scatter is slightly increased, but the correlation is significantly greater. These plots are typical for the overlap regions.

3.4 External check with APM Sky Catalogue data

In order to check our results further, we performed an external test for similar alignments in APM data[†] in order to test for any systematic effects introduced by the SuperCOSMOS scanning procedure. We took a J-R paired star/galaxy

[†] available on <http://www.ast.cam.ac.uk/~mike/apmcat/>

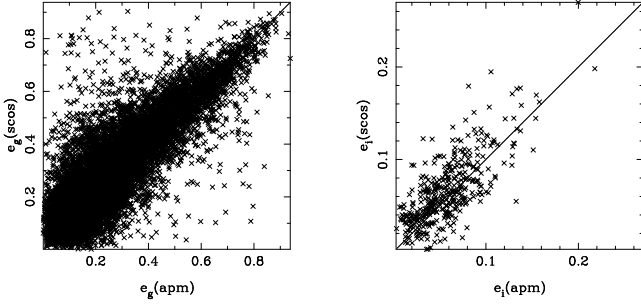


Figure 5. LHS: Scatter plot of the SuperCOSMOS galaxy ellipticities on a plate against those from the APM galaxy survey. RHS: The same as the LHS but for binned cells.

catalogue from the APM survey for one field and paired it up with the SuperCOSMOS data. Although the weighting for galaxy shapes is different, being density rather than intensity weighted, the magnitude cut is low enough that the difference should not matter.

Figure 5 shows a scatter plot for individual galaxy ellipticities for a plate on both SuperCOSMOS and APM surveys, and for the binned data, indicating a strong agreement between the surveys. Having checked for internal and external consistency in the ellipticity catalogue, we now turn to estimating the variance of the ellipticities in cells of varying scale, across all of the plates.

3.5 Estimator for the ellipticity variance

The variance of the cell ellipticities can be expressed as the sum of the contributions from all possible sources of alignment (e.g. Bacon et al., 2000)

$$\sigma_{tot}^2 = \sigma_{lens}^2 + \sigma_{int}^2 + \sigma_{noise}^2 + \sigma_{sys}^2 \quad (6)$$

where we have included the contributions from lensing, intrinsic alignments, shot noise and systematics. We assume in what follows that the lensing signal is negligible compared to that from intrinsic alignments for the median redshift of the galaxies in our sample ($z \approx 0.1$). The noise term, σ_{noise}^2 is due to intrinsic scatter in galaxy ellipticities and the random error in the measurement of the galaxy ellipticities. Per cell this error is large, as indicated by the large scatter about a small offset in the right-hand-plot of Figure 2. However, since we are averaging over a very large area of sky (196 plates covering ≈ 5000 sq. degrees with $\approx 1.7 \times 10^6$ galaxies), we can expect to beat this term down statistically. The final term in equation (6) is due to systematic sources of error. In Section 3.3 we demonstrated the internal consistency of the catalogue, indicating that contributions to this term from variations in the catalogue are small. Further tests are presented in Section 4.2

We have used a minimum variance estimator for the intrinsic ellipticity variance, σ_{int}^2 due to intrinsic alignments in excess of the noise,

$$\sigma_{int}^2 = \frac{\sum_i w_i (e_i^2 - \mathcal{N}_i)}{\sum_i w_i} \quad (7)$$

where \mathcal{N}_i is the random noise on the estimated cell ellipticity, e_i , in the i^{th} cell, and w_i is an arbitrary weighting factor. We assume that the mean cell ellipticity components are zero

(see Section 4.2). For the moment we will ignore systematic terms.

Our aim here is to use the measured uncertainty on the ellipticity of each cell as an estimate of the noise component of the variance, assuming it is dominated by random errors. The uncertainty on the ellipticity of each cell is given by

$$\sigma^2(\bar{e}_{\alpha,i}) = \frac{1}{N-1} \sum_{j=1}^N (e_{\alpha,j} - \bar{e}_{\alpha,i})^2, \quad \alpha = 1, 2, \quad (8)$$

where N is the number of galaxies in the cell. The random noise term per cell is then estimated by the random variance per galaxy, divided by the number of galaxies per cell;

$$\mathcal{N}_i = \frac{1}{e_i^2 N} [\bar{e}_{1,i}^2 \sigma^2(\bar{e}_{1,i}) + \bar{e}_{2,i}^2 \sigma^2(\bar{e}_{2,i})]. \quad (9)$$

For a minimum variance estimator, we wish to choose the weights, w_i such that equation (7) is minimised with respect to w_i . This optimal weighting scheme is given by

$$w_i = [\sigma^2(e_i^2) + \sigma^2(\mathcal{N}_i)]^{-1} = (4e_i^2 \mathcal{N}_i + 2\mathcal{N}_i^2)^{-1}, \quad (10)$$

where $\sigma^2(e_i^2)$ is the uncertainty on the measured total ellipticity variance, and $\sigma^2(\mathcal{N}_i)$ is the uncertainty on the estimated noise term. The value of $\sigma^2(e_i^2)$ is given by $\sigma^2(e_i^2) = 4e_i^2 \mathcal{N}_i$. The uncertainty in the noise term can be estimated by noting that the noise contribution from randomly orientated galaxies will be $\mathcal{N}_i = e_{rms}^2/N$ where e_{rms} is the root mean squared random ellipticity of the galaxies. The variance of the noise is then given by $\sigma^2(\mathcal{N}_i) = \langle e_g^4 \rangle / N^2 - e_{rms}^4 / N^2$ where e_g is the ellipticity of the individual galaxies in cell i . Assuming a Gaussian distribution for the galaxy ellipticities, we can make the approximation, $\langle e_g^4 \rangle \approx 3\langle e^2 \rangle^2 = 3e_{rms}^4$ and we have $\sigma^2(\mathcal{N}_i) = 2e_{rms}^4 / N^2 = 2\mathcal{N}_i^2$. Combining these variances yields the weighting in equation (10). Substituting this into the expression for σ_{int}^2 yields the minimum variance estimator:

$$\sigma_{int}^2 = \frac{\sum_i (e_i^2 - \mathcal{N}_i) / (4e_i^2 \mathcal{N}_i + 2\mathcal{N}_i^2)}{\sum_i (4e_i^2 \mathcal{N}_i + 2\mathcal{N}_i^2)^{-1}}. \quad (11)$$

The error in this expression is given by

$$\sigma^2(\sigma_{int}^2) = \frac{1}{\sum_i w_i} = \left(\sum_i (4e_i^2 \mathcal{N}_i + 2\mathcal{N}_i^2)^{-1} \right)^{-1}. \quad (12)$$

Equations (11) and (12) form the basis of our analysis.

4 RESULTS

4.1 Measurement of the galaxy ellipticities

We have used equation (11) to calculate the variance of the intrinsic cell ellipticities, σ_{int}^2 over a wide range of angular scales. The results of these measurements are shown in Figure 6. The signal drops sharply for angular scales ≥ 10 arcmins ($\approx 1 h^{-1}$ Mpc) which is expected for both weak lensing and intrinsic alignments. However, our measurements are two order of magnitudes larger than the signal expected from weak lensing (see e.g. Jain & Seljak, 1997) for a median source redshift of $z \approx 0.1$ corresponding to the magnitude cut of $b_J \leq 20.5$ which we have used in our analysis. In Figure 6 we plot our results along with the predicted weak lensing signal for a cluster normalised Λ CDM model, with

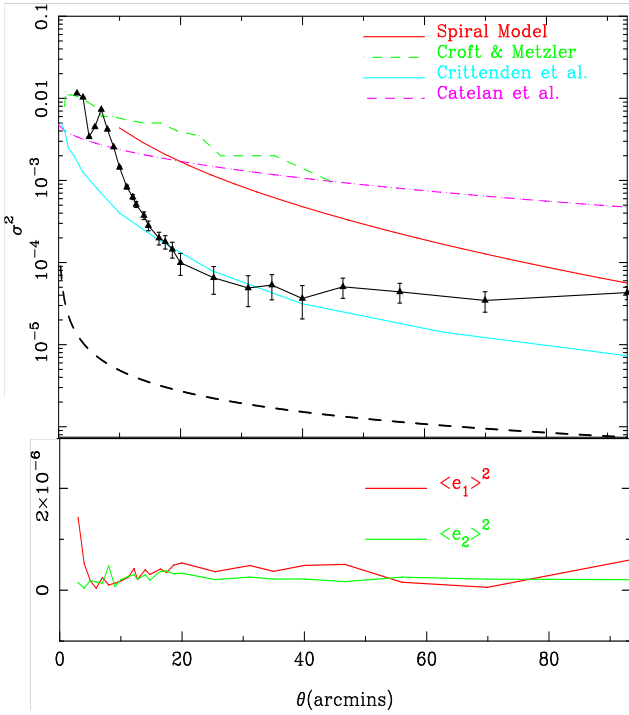


Figure 6. Top panel: Measured ellipticity variance, σ_{int}^2 (triangles) over 196 SGC fields as a function of angular scale, θ along with the weak lensing prediction (heavy dashed line) for a Λ CDM model and a median redshift equal to that of our galaxy sample. Also shown are various predictions for the intrinsic signal - see text for details. Bottom panel: Cell ellipticities averaged over the entire survey.

$\Omega_m = 0.3$ and $\Omega_\Lambda = 0.7$. The discrepancy is exhibited over the entire range of angular scale, θ suggesting that we have not measured extrinsic gravitational lensing.

4.2 Tests for systematics

To test our results for internal systematics we have estimated the means of the cell ellipticity components averaged over all plates. In Figure 6 we show that the mean fields are negligible ($\langle e_\alpha \rangle^2 < 10^{-7}$) on all scales. We have also estimated the star-galaxy covariance,

$$\langle ee^* \rangle = \langle e_1 e_1^* \rangle + \langle e_2 e_2^* \rangle, \quad (13)$$

where e^* is the stellar ellipticity. This is shown in Figure 7, and is well below our results ($|\langle ee^* \rangle| < 10^{-5}$) on all scales, indicating that our correction scheme for ellipticities does not correlate galaxies with stars. We also estimated the cross-correlation of e_1 and e_2 for the galaxies, $\langle e_1 e_2 \rangle$. This is also plotted in Figure 7 and again shows no significant correlation ($|\langle e_1 e_2 \rangle| < 10^{-5}$). We have also tested our estimator (equation 11) by randomising the galaxy ellipticities. An ellipticity variance well below the signal is measured on all scales from the randomised galaxies (Figure 7). Finally, as an external test of systematics we have pushed the APM data (Section 3.4) through our analysis for one plate. Figure 7 shows the measured ellipticity variances for both the SuperCOSMOS and APM surveys, for a single plate. Again we find a very good agreement between both catalogues,

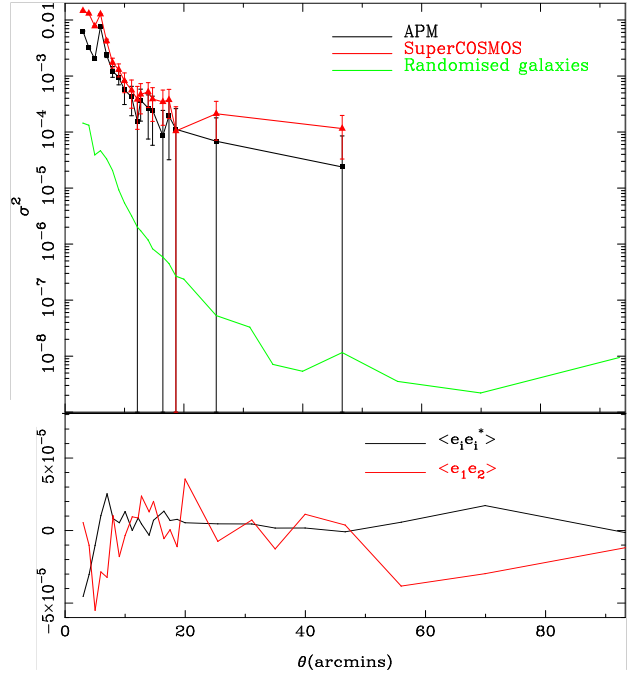


Figure 7. Top panel: Comparison of the SuperCOSMOS variance of ellipticities and the APM variance for one plate (UKST field 78). Also plotted is the signal measured from the randomised dataset (see Section 4.2). Bottom panel: The star-galaxy covariance and the galaxy cross correlation as described in the text.

suggesting that any systematic effects in our analysis are small, $\sigma_{sys}^2 < 10^{-5}$, and below our measurement.

4.3 Intrinsic alignments

Recent numerical and analytic studies (Catelan et al., 2000; Crittenden et al., 2000; Croft & Metzler, 2000; Heavens et al., 2000) have put constraints on the shear signal expected from intrinsic galaxy alignments. In these studies the galaxy shape is estimated either from the perpendicular to the halo angular momentum vector for spirals, or from the shape of the halo for ellipticals.

In Figure 6 we have plotted our results along with the alignment effect estimated from each group. Also shown are results from numerical simulations for a spiral galaxy model at $z = 0.1$ (A. Heavens, private communication). The spread in models can be accounted for by the choice of mechanism and galaxy type, assumptions about alignments between halos and galaxies, correlations between tidal and inertial fields and disc thicknesses. We have used the redshift scaling z^{-2n} , suggested by Crittenden et al., where n is the slope of the matter correlation function, to scale the results from different redshifts. We have also assumed $\sigma^2(\theta) = 2/(2-n)C(\theta)$, where $C(\theta)$ is the ellipticity correlation function.

Generalising the arguments by Crittenden et al. (2000), at large scales the ellipticity variance should scale as

$$\sigma^2(\theta) \approx Az^{-2n} |1 + (\theta/\theta_0)^2|^{-n}. \quad (14)$$

Since our results show that the variance is roughly independent of scale, this implies that the matter correlation function must be roughly constant on scales $> 4h^{-1}$ Mpc. This is in marked contrast to the galaxy correlation func-

tion, which scales as $n = -1.8$. This may indicate that on small scales the clustering pattern of galaxies is different to that of dark matter.

5 CONCLUSION

In this letter we have presented a measurement of the intrinsic alignment effect of galaxies on scales from a few arcminutes to 100 arcminutes. Using 1.7 million galaxy ellipticities measured from the digitized SuperCOSMOS Sky Survey, to a depth of $b_J = 20.5$ and median redshift $z = 0.1$ and covering 196 plates or 5000 sq. deg., we have corrected the data for plate distortions and seeing, and applied a new minimum variance estimator to the data.

After correcting for distortions and seeing, we find our measurements are internally consistent, with good agreement in regions where the plates overlap, with effectively zero star-galaxy ellipticity correlations and zero e_1 - e_2 cross-correlations. We have also demonstrated external consistency with the APM sky catalogue data over a restricted region of sky, indicating that we are not contaminated by measurement systematics. We have tested our estimator by randomising the galaxy ellipticities in the catalogue and applying the analysis to the resulting data. The effectively zero shear variance measured from the randomised catalogue shows that our estimator is unbiased.

Our resulting estimates of the ellipticity variance over a wide range of scales are two orders of magnitude higher than that expected from gravitational lensing by large-scale structure, but roughly in line with those predicted from intrinsic alignments in the gravitational instability scenario, although the predictions for intrinsic alignments are still uncertain. For instance, it is not clear if the effect is dominated by tidal spin or shape alignments. This agreement suggests that we are not contaminated by internal systematics.

Our results imply that other shallow surveys, such as the Sloan Digital Sky Survey, should measure roughly the same contribution to the total variance from intrinsic alignments and gravitational lensing shear. Since the intrinsic alignment signal is expected to scale as z^{-2} (Crittenden et al., 2000) and the lensing signal as $z^{1.5}$ (Jain & Seljak, 1997), we expect the ratio of intrinsic alignment to gravitational shear to scale as

$$\frac{\sigma_{int}^2}{\sigma_{lens}^2} \approx 10^2 \left(\frac{z}{0.1} \right)^{-3.5}. \quad (15)$$

This ratio is unity at around $z \approx 0.37$. Higher redshift surveys, such as the VISTA Gravitational Lensing Survey (Taylor 2000, in prep.) with $z \approx 1$, will measure gravitational lensing shear.

While one would hope that the correlations between ellipticity, spin and the shear field would allow one to measure the amplitude of the dark matter density field, the spin is also determined by the inertial tensor of the dark matter halo. At present, the relation between shape and the local shear field of haloes, and the relationship between galaxy ellipticity and halo shape, introduces a large uncertainty in our understanding of intrinsic ellipticity alignments. However, the flatness of the measured variance of alignments suggests that the matter correlation function is very flat, in contrast to the observed galaxy correlation function. With

present and future observations and theory we can hope to resolve these issues.

ACKNOWLEDGEMENTS

MLB thanks the University of Edinburgh for a studentship. SD thanks the PPARC for a PDRA grant, and the Institute for Astronomy, Edinburgh for support during the writing of this paper. ANT is a PPARC Advanced Fellow. MLB and ANT thank Alan Heavens and Rob Crittenden for useful discussion about intrinsic alignment effects. The authors thank the Institute for Astronomy's Wide Field Astronomy Unit for assistance in this project.

REFERENCES

- Bacon D., Refregier A., Ellis R., 2000, submitted MNRAS (astro-ph/0003008)
- Bartlemann M., Schneider P., 1999, Review for Physical Reports (astro-ph/9909155)
- Catelan P., Kamionkowski M., Blandford R.D., 2000, submitted to MNRAS (astro-ph/0005470)
- Crittenden R., Natarajan P., Pen-U., Theuns T., 2000, submitted to ApJ (astro-ph/0009052)
- Croft R.A.C., Metzler C.A., 2000, submitted to ApJ (astro-ph/0005384)
- Heavens A.F., Refregier A., Heymans C., 2000, submitted to MNRAS (astro-ph/0005269)
- Hambly N.C., et al., 2000a, in preparation
- Hambly N.C., Irwin M.J., MacGillivray H.T., 2000b, in preparation, available on <ftp://ftp.roe.ac.uk/nch/pub/paper2.ps.gz>
- Hoyle, F., 1949, in Burgers J.M., van de Hulst H.C., eds., in Problems of Cosmic Aerodynamics, Central Air Documents, Dayton, Ohio, p195
- Jain B., Seljak U., 1997, ApJ, 484, 560
- Kaiser N., Wilson G., Luppino G., 2000, submitted to ApJL (astro-ph/0003338)
- Pen U-L., Lee J., Seljak U., 2000, submitted to the ApJL (astro-ph/0006118)
- van Waerbeke L., et al, 2000, submitted to A&A (astro-ph/0002500)
- Wittman D.M., Tyson J.A, Kirkman D., Dell'Antonio I., Bernstein G., 2000, Nature, 405, 143